A Study on the Temperature Dependence of the Ginzburg-Landau Parameter, Thermodynamic and Upper Critical Field of Nb_3Sn Strands

Sangjun Oh, D. K. Oh, C. J. Bae, H. C. Kim, and Keeman Kim

***Abstract*—We report detailed magnetization measurement results for two internal-tin Nb_3Sn strands. The paramagnetic background of a Mitsubishi strand is about 4 times larger than that of a KAT strand below the transition temperature, which can be understood as combined effects of Pauli and Langevin paramagnetism. From magnetic relaxation measurement for the KAT strand, a possibility of surface barrier effect is discussed. After subtracting the paramagnetic background, reversible magnetization data are analysed using the Hao-Clem model and the Ginzburg-Landau parameters (κ), the thermodynamic and the upper critical fields (B_c, B_{c2}) at various temperatures are obtained. The temperature dependences of κ, B_c and B_{c2} are compared with the recent theoretical calculation results for Nb_3Sn and also with widely used empirical formulas.**

***Index Terms*—Eliashberg theory, paramagnetic background, superconducting parameters, the Hao-Clem model.**

I. Introduction

On a proper scaling law especially for the critical current of Nb_3Sn strands, there is a growing interest, however, no consensus yet. In general, proposed scaling laws state that the pinning force can be represented as a function of the Ginzburg-Landau parameter (κ) and the upper critical field (B_{c2}) [1]–[6]. In Ekin-Summer's scaling law, the Summers approximate expression for the temperature dependence of κ is used $\kappa(T) = \kappa(0)[1 - 0.31t^2(1 - 1.77\ln t)]$, where t is a ratio of temperature to the critical temperature, $t = T/T_c$. The temperature dependence of the thermodynamic critical field (B_c) is usually described by $B_c(T) = B_c(0)(1 - t^2)$, following the two fluid model approximation. From the definition of κ, the temperature dependence of $B_{c2}(T)$ can be written as a product of κ and B_c, $B_{c2}(T) = \sqrt{2}\kappa(T)B_c(T)$ [1]. These temperature dependences are also used in the deviatoric strain scaling law of ten Haken and his co-workers [2]. Recently, Taylor *et al.* [5] and Godeke *et al.* [6] reported that $B_{c2}(T)$ can be better approximated by $B_{c2}(T) = B_{c2}(0)(1 - t^v)$, where ν is about 1.5 and in their scaling laws, $\kappa(T)$ is represented as a ratio of $B_{c2}(T)$ to $B_c(T)$, instead. In our previous work, the results of theoretical calculations for Nb_3Sn using strong coupling theory of superconductors (Eliashberg theory) were reported [4]. It was shown that $B_c(T)$ can be better described by $B_c(T) = B_c(0)(1-t^{2.17})$ and also argued that the Summers relation, $\kappa(T)$, shows deviation from the calculation results.

The Summers expression or the recent $B_{c2}(T) = B_{c2}(0)(1-t^v)$ relation were obtained from the analysis of the critical current measurements, except the work of Godeke *et al.* [7], where the $B_{c2}(T)$ relation is obtained by direct transport measurements. In this work, we report on the temperature dependences of $\kappa(T)$, $B_c(T)$ and $B_{c2}(T)$ from magnetization measurements. In Section II, it is shown that the paramagnetic backgrounds are quite significant near the critical temperature and are strongly sample dependent. The reversible magnetization data are analysed using the Hao-Clem model and the obtained temperature dependences of κ, B_c and B_{c2} are discussed in Section III.

II. Paramagnetic Background

Two internal-tin processed Nb_3Sn strands are used for the measurements. A Mitsubishi (MELCO: Mitsubishi Electric Corporation) strand has been used for the construction of the KSTAR (Korea Superconducting Tokamak Advanced Research) superconducting magnet system. The strain dependences of the critical currents for the MELCO strand and a KAT (Kiswire Advanced Technology) strand at 4.2 K had been reported elsewhere [8]. The length of the sample used for the measurement is 10 mm for the MELCO strand and 5 mm for the KAT strand (KAT B strand in [8]). To reduce the demagnetization effect, both strands are mounted along with the direction of field during the measurements. Magnetizations are measured with a Quantum Design MPMS (Magnetic Properties Measurement System) SQUID magnetometer. The magnetic relaxations are measured with a Quantum Design PPMS (Physical Properties Measurement System) with ACMS (AC Measurement System) option, which enables faster measurements.

Fig. 1 shows typical hysteresis measurement results for both strands at 15.5 K. At high field, the magnetization curves are reversible and the paramagnetic contributions, probably caused by non-superconducting elements other than Nb_3Sn in the strands, are obvious. The curvature observed in the high field region of the hysteresis curve for the MELCO strand is a typical feature we can expect for Langevin paramagnetism. Fig. 2 is the temperature dependence of magnetization for the MELCO strand with an applied field of 500 Oe. It can be understood as a sum of a temperature independent Pauli paramagnetism contribution, which is represented as a horizontal dotted line in Fig. 2, and

Manuscript received August 29, 2006. This work was supported by the Korea Ministry of Science and Technology.

The authors are with the National Fusion Research Center, Daejeon 305-333, Korea (e-mail: wangpi@nfrc.re.kr).

Color versions of one or more of the figures in this paper are available online at http://ieeexplore.ieee.org.

Digital Object Identifier 10.1109/TASC.2007.899368

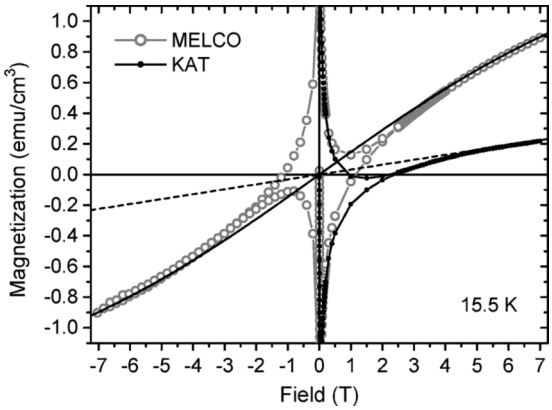

Fig. 1. The magnetization measurement results for the MELCO and the KAT strand at 15.5 K. Solid line is a sum of linear Pauli paramagnetic background and Langevin paramagnetic effect calculated with (1). Dotted line is a linear calculated background using the susceptibility with (2).

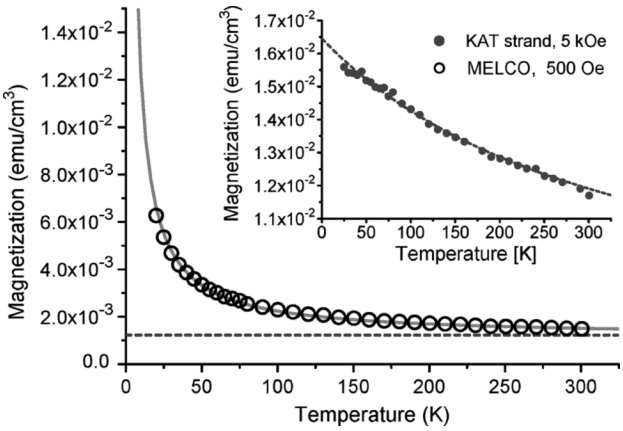

Fig. 2. The temperature dependence of magnetization for the MELCO strand with applied field of 500 Oe. Dotted line is a fitted temperature independent Pauli paramagnetic background and solid line represents the Langevin paramagnetism calculated with (1). *Inset*: The temperature dependence of magnetization for the KAT strand with applied field of 5 kOe. Dotted line is calculated with (2).

Langevin paramagnetic effect, the solid line in Fig. 2. The Solid line is fitted with the following Brillouin function [9],

$$M = NgJ\mu_B B_J(x), \quad (x \equiv gJ\mu_B B/k_B T)$$
$$B_J(x) = \frac{2J+1}{2J} ctnh\left(\frac{(2J+1)x}{2J}\right) - \frac{1}{2J} ctnh\left(\frac{x}{2J}\right) \quad (1)$$

After subtracting the contribution of Pauli paramagnetic background, the magnetization curves as a function of B/T at various temperatures around the critical temperature are shown in Fig. 3. Solid lines in Figs. 2 and 3 are calculated with (1) using parameters, $g = 1.86$, $J = 5/2$. Above the transition temperature, magnetization measurement results coincide with the calculated fitting line.

On the other hand, the paramagnetic backgrounds in the hysteresis curves for the KAT strand are simply linear and the paramagnetic susceptibility shows weak temperature dependence as can be seen in the inset of Fig. 2. The inset of Fig. 2 is the magnetization as a function of temperature for the KAT strand at

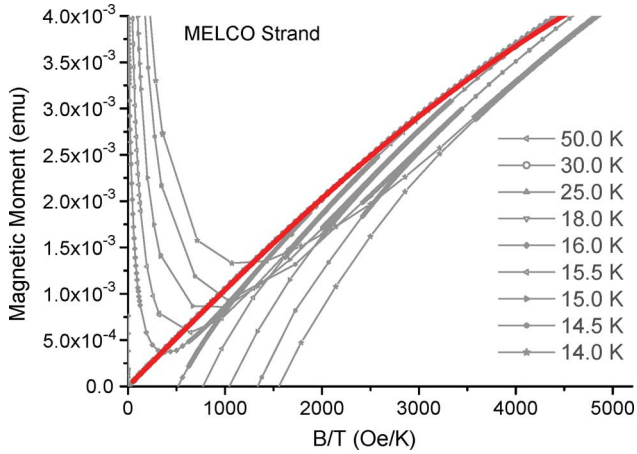

Fig. 3. The magnetization plots with B/T at various temperatures after subtracting the Pauli paramagnetic backgrounds. Solid line is calculated with (1) with parameters, $g = 1.86$, $J = 5/2$.

5 kOe. The paramagnetic background susceptibility χ for the KAT strand can be written as,

$$\chi = 1.33 \times 10^{-5} + 6.76 \times 10^{-5}/(T + 345.3). \quad (2)$$

Both the MELCO and the KAT strands are fabricated by internal-tin method and the diameters are both 0.778 mm, a similar non-Cu fraction of 0.4 and 0.5, respectively, and were heat treated by the same heat treatment scenarios. It is quite interesting that the small difference in the ternary contents or in the sample geometry result in such a huge difference in the paramagnetic backgrounds.

III. The Hao-Clem Model Analysis and the Temperature Dependences of κ, H_c and H_{c2}

Fig. 4 are the magnetization hysteresis curves for the KAT strand at various temperatures below the transition temperature, after subtracting the paramagnetic backgrounds discussed in Section II. The thermodynamic parameters, such as the thermodynamic critical field (B_c), can be determined from the reversible magnetization. As can be seen in Fig. 4, the magnetization is irreversible below a certain field (this field is usually defined as the irreversibility field, B_{irr}) even at 16.5 K. If this irreversibility is only due to the bulk pinning effect then the magnetic relaxation rates will be the same for the field increasing branch and the decreasing branch. The reversible magnetization can be approximated as a mean value of the magnetizations in the field increasing branch and the decreasing branch. However, the magnetic relaxations are quite different as shown in the inset of Fig. 4. The inset of Fig. 4 is the relaxation measurement results for the KAT strand at 14 K, with an applied field of 5 kOe. The data represented as solid squares are measured in the increasing field branch and the open circles in the decreasing field branch. The magnetic relaxation in the field increasing branch shows a typical logarithmic decay, while the relaxation in the decreasing branch appear to be strongly non-linear as a function of time. A possible explanation for this difference in the relaxation rate is the Bean-Livingston surface barrier [10]. In

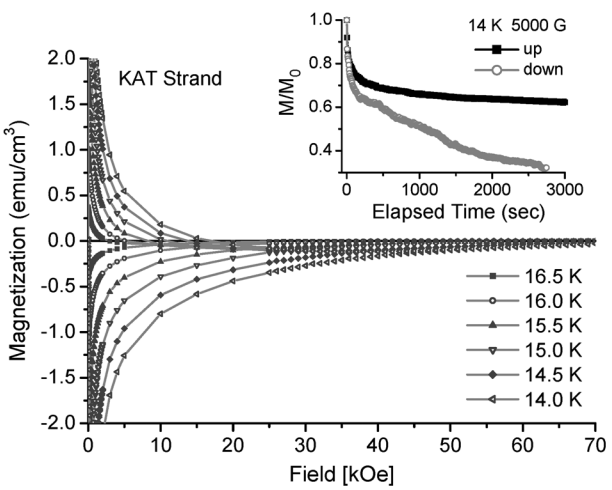

Fig. 4. The magnetization results for the KAT strand at various temperatures after subtracting the paramagnetic backgrounds. Inset: Magnetic relaxation measurements for the KAT strand at 14 K and 5 kOe.

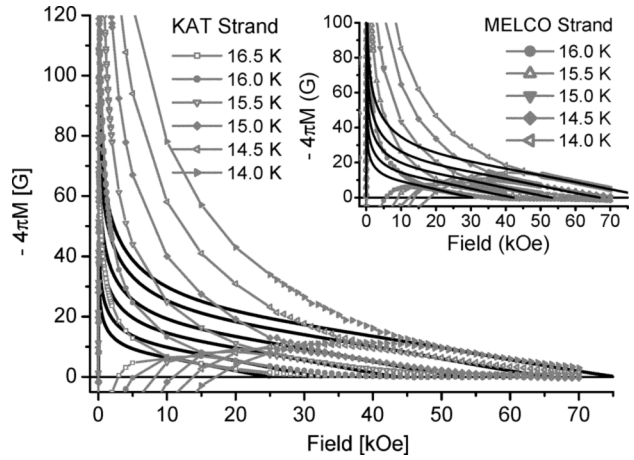

Fig. 5. The (superconducting) volume magnetizations for the KAT strand at various temperatures. Solid lines are the Hao-Clem fitting results. *Inset*: The volume magnetizations for the MELCO strand with the Hao-Clem fitting results.

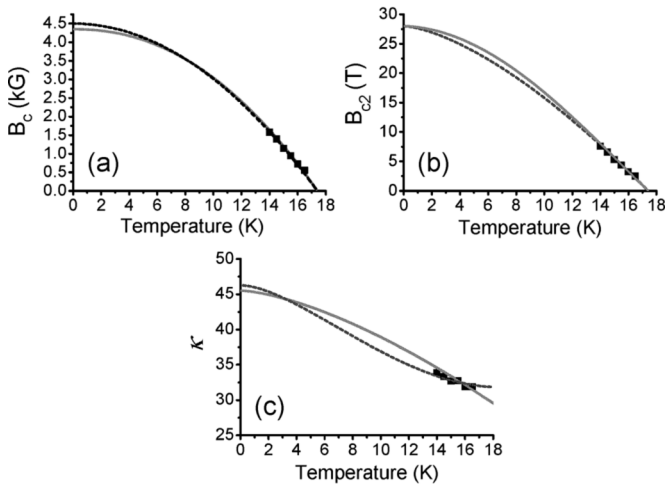

Fig. 6. The temperature dependences of the superconducting parameters obtained from the Hao-Clem model analysis for the KAT strand. Solid lines are calculated with (3). Dotted lines are calculated with empirical formulas.

the presence of surface barrier, asymmetry in the relaxation rate for flux entry and exit was predicted.

Due to the possibility of surface barrier, only the magnetization data above the irreversibility field are analysed. For the analysis, the Hao-Clem model is applied [11]. In the Hao-Clem model, a trial function with two parameters for the order parameter is assumed to solve the Ginzburg-Landau equations. The two variational parameters ξ_v and f_∞, represent the finite size of a vortex core and the reduction of the order parameter by vortices overlap, respectively. The free energy including the core energy as well as the energy of the circulating currents is minimized with respect to these variables. It is widely used for the description of the reversible magnetization and for the determination of the thermodynamic parameters of type-II superconductors [12]. Fig. 5 shows the volume magnetizations as a function of field at various temperatures with the Hao-Clem fitting results. For the Hao-Clem fitting, the magnetization data shown in Fig. 4 are normalized by the superconducting volume fraction. The superconducting volume fraction is obtained from the initial slope below the lower critical field (B_{c1}) where the perfect diamagnetism is expected. The non-Cu fraction for the KAT strand is 0.5 and the superconducting volume fraction with respect to the non-Cu volume at 16.5 K is 14.3%. The superconducting volume fraction sharply increases with decreasing temperature. It is 22.8% and 24.5%, at 15.5 and 15 K respectively and finally saturated below 14.5 K to 25.7%. Similar behavior is observed for the MELCO strand. At 16 K the superconducting volume fraction is 20.4% and saturated to 25.5% below 14.5 K. Near the upper critical field, a slight positive curvature is observed in the $-4\pi M$ data shown in Fig. 5. It is attributed to sample inhomogeneity and the $-4\pi M$ data lower than 5 G are not used for the fitting.

The temperature dependences of the Ginzburg-Landau parameter (κ), the thermodynamic and the upper critical field (B_c, B_{c2}) obtained from the Hao-Clem analysis for the KAT and the MELCO strand are shown in Figs. 6 and 7. According to the recent theoretical calculations for Nb_3Sn using strong coupling theory of superconductors, the temperature dependences of superconducting parameters can be written as [4],

$$\begin{aligned} B_c(T) &= B_c(0)(1-t^{2.17}), \quad t = T/T_c \\ \kappa(T) &= \kappa(0)\left(1+u(1-t^v)\right)/(1+u) \\ B_{c2}(T) &= B_{c2}(0)(1-t^{2.17})\left(1+u(1-t^v)\right)/(1+u) \end{aligned} \quad (3)$$

Solid lines in Figs. 6 and 7 are calculated with (3). The fitting parameters, $B_c(0)$, $B_{c2}(0)$, $\kappa(0)$, T_c, u, and v, for the KAT strand are 4.35 kG, 28.0 T, 45.5, 17.4 K, 0.5, 1.5 and for the MELCO strand, 5.05 kG, 32.0 T, 44.8, 17.0 K, 0.5, 1.5, respectively. The differences in the superconducting parameters between the KAT and the MELCO strands can be attributed to slight differences in tin content or ternary element addition. The effects of tin content variation and ternary element on T_c and $B_{c2}(0)$ are recently reviewed by Godeke [13].

Dotted lines in Figs. 6 and 7 are calculated with widely used empirical formulas, for comparison. For the temperature dependence of B_c, the two fluid model approximation, $B_c(T) =$

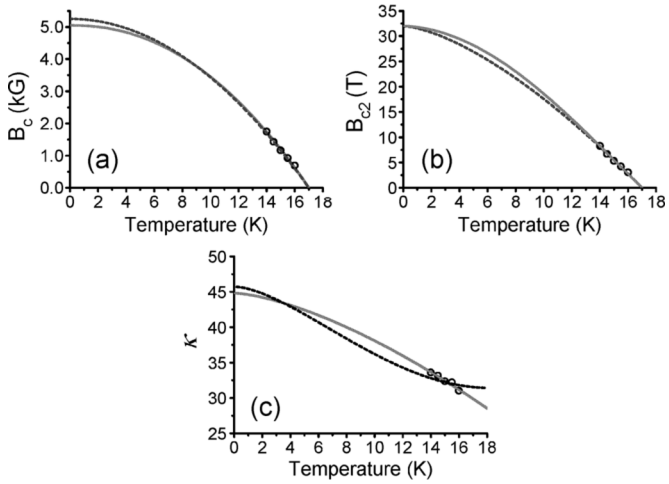

Fig. 7. The temperature dependences of the superconducting parameters obtained from the Hao-Clem model analysis for the MELCO strand. Solid lines are calculated with (3). Dotted lines are calculated with empirical formulas.

$B_c(0)(1-t^2)$, is represented as a dotted line in Figs. (6a) and (7a). The best fit is obtained with $B_c(0)$ of 4.5 kG for the KAT strand and 5.25 kG for the MELCO strand, with the same value of T_c used for the fitting with (3). $B_c(0)$ obtained from the fitting to the empirical formula is slightly higher than that obtained from the fit to (3). In Figs. (6b) and (7b), an empirical expression for the temperature dependence of the upper critical field [5], [6], $B_{c2}(T) = B_{c2}(0)(1-t^v)$, with $\nu = 1.5$ is shown as a dotted line. The same fitting parameters of T_c and $B_{c2}(0)$ obtained from the fit to (3) are used. The empirical relation for $B_{c2}(T)$ is also reported by Godeke *et al.* [7] from the analysis of resistive transition data. In their work, the upper critical fields obtained from transport measurements are reported to be comparable with magnetization results where the B_{c2} is defined as the lowest field at which magnetization without paramagnetic background becomes zero. The Summers relation [1], $\kappa(T) = \kappa(0)[1 - 0.31t^2(1 - 1.77\ln t)]$, is presented as a dotted line in Figs. (6c) and (7c). The fitting parameter $\kappa(0)$ used for the calculation of the Summers expression are 46.3 for the KAT strand and 45.7 for the MELCO strand. Within the temperature range analysed in this work, it is difficult to verify the validity of a particular expression. The lower bound of 14 K is due to the magnetic field limitation of the SQUID magnetometer. Below 14 K, the irreversibility fields are very close to or even higher than 7 T, the maximum field used in this work, and the Hao-Clem model analysis cannot be applied. With a bit lower temperature and higher field measurements, a proper expression especially for the Ginzburg-Landau parameter might be easily verified. If we can further determine the strain dependences of the superconducting parameters from magnetization measurements by the method described in this work, the strain and temperature dependences proposed in each scaling law can be directly compared.

IV. Conclusion

In Summary, detailed magnetization measurements for two internal-tin Nb_3Sn strands have been made. A huge difference in paramagnetic backgrounds for the two strands is observed. In particular, the paramagnetic background for the MELCO strand can be represented as a sum of Pauli and Langevin paramagnetism. From the asymmetry in the magnetic relaxation rate for flux entry and exit, we report a possibility of surface barrier effect. Reversible magnetization data are analysed by the Hao-Clem model to deduce the temperature dependences of the Ginzburg-Landau parameters (κ), the thermodynamic and the upper critical fields (B_c, B_{c2}). The temperature dependences of the superconducting parameters obtained are compared with the recent theoretical predictions and the empirical formulas. The method used in this work will be useful for a study on the strain and temperature dependences of the superconducting parameters from magnetization measurements.

References

[1] L. T. Summers, M. W. Guinan, J. R. Miller, and P. A. Hahn, "A model for the prediction of Nb_3Sn critical current as a function of field, temperature, strain, and radiation damage," *IEEE Trans. Magnetics*, vol. 27, no. 2, pp. 2041–2044, Mar. 1991.

[2] B. ten Haken, A. Godeke, and H. H. J. ten Kate, "The strain dependence of the critical properties of Nb_3Sn conductors," *J. Appl. Phys.*, vol. 85, pp. 3247–3253, Mar. 1999.

[3] S. A. Keys and D. P. Hampshire, "A scaling law for the critical current density of weakly- and strongly-coupled superconductors, used to parameterize data from a technological Nb_3Sn strand," *Supercond. Sci. Technol.*, vol. 16, pp. 1097–1108, Aug. 2003.

[4] S. Oh and K. Kim, "A scaling law for the critical current of Nb_3Sn stands based on strong-coupling theory of superconductivity," *J. Appl. Phys.*, vol. 99, p. 033909, Feb. 2006.

[5] D. M. J. Taylor and D. P. Hampshire, "The scaling law for the strain dependence of the critical current density in Nb_3Sn superconducting wires," *Supercond. Sci. Technol.*, vol. 18, pp. S241–S252, Nov. 2005.

[6] A. Godeke, B. ten Haken, H. H. J. ten Kate, and D. C. Larbalestier, "A general scaling relation for the critical current density in Nb_3Sn," *SuperCond. Sci. Technol.* [Online]. Available: arXiv:cond-mat/0608404 v1, to be published

[7] A. Godeke, M. C. Jewell, C. M. Fischer, A. A. Squitieri, P. J. Lee, and D. C. Larbalestier, "The upper critical field of filamentary Nb_3Sn conductors," *J. Appl. Phys.*, vol. 97, p. 093909, 2005.

[8] S. Oh, S. H. Park, C. Lee, Y. Chang, K. Kim, and P.-Y. Park, "A strain dependence of critical current in internal Tin process Nb_3Sn strands," *IEEE Trans. Appl. Supercond.*, vol. 15, pp. 3462–3465, Jun. 2005.

[9] C. Kittel, *Introduction to Solid State Physics*. New York: John Wiley & Sons, 1996, ch. 14.

[10] Y. Yeshurun, A. P. Malozemoff, and A. Shaulov, "Magnetic relaxation in high-temperature superconductors," *Rev. Mod. Phys.*, vol. 68, no. 3, pp. 911–949, Jul. 1996.

[11] Z. Hao, J. R. Clem, M. W. McElfresh, L. Civale, A. P. Malozemoff, and F. Holtzberg, "Model for the reversible magnetization of high-κ type-II superconductors: Application to high- T_c superconductors," *Phys. Rev. B*, vol. 43, pp. 2844–2852, 1991.

[12] W. V. Pogosov, K. I. Kugel, A. L. Rakhnov, and E. H. Brant, "Approximate Ginzburg-Landau solution for the regular flux-line lattice: Circular cell method," *Phys. Rev. B*, vol. 64, p. 064517, 2001.

[13] A. Godeke, "A review of the properties of Nb_3Sn and their variation with A15 composition, morphology and strain state," *Supercond. Sci. Technol.*, vol. 19, pp. R68–R80, Jun. 2006.